Spin Fano Resonances and Control in Two-Dimensional Mesoscopic Transport

Chen-Rong Liu, Liang Huang, Honggang Luo, and Ying-Cheng Lai

Phys. Rev. Applied **13**, 034061 — Published 25 March 2020

DOI: 10.1103/PhysRevApplied.13.034061

Spin Fano resonances and control in two-dimensional mesoscopic transport

Chen-Rong Liu,[1] Liang Huang,[1,*] Honggang Luo,[1,2] and Ying-Cheng Lai[3,4]

[1] *School of Physical Science and Technology, and Key Laboratory for Magnetism and Magnetic Materials of MOE, Lanzhou University, Lanzhou, Gansu 730000, China*

[2] *Beijing Computational Science Research Center, Beijing 100084, China*

[3] *School of Electrical, Computer, and Energy Engineering, Arizona State University, Tempe, AZ 85287, USA*

[4] *Department of Physics, Arizona State University, Tempe, AZ 85287, USA*

In electronic transport through mesoscopic systems, the various resonances in quantities such as conductance and scattering cross sections are characterized by the universal Fano formula. Does a similar formula exist for spin transport? We provide an affirmative answer by deriving a Fano formula to characterize the resonances associated with two fundamental quantities underlying spin transport: spin-resolved transmission and spin polarization vector. In particular, we generalize the conventional Green's function formalism to spin transport and use the Fisher-Lee relation to obtain the spin resolved transmission matrix, which enables the spin polarization vector to be calculated, leading to a universal Fano formula for spin resonances. Particularly, the theoretically obtained resonance width depends on the nature of the classical dynamics as determined by the geometric shape of the dot. We explicitly demonstrate this fact and argue that it can be exploited to smooth out or even eliminate Fano spin resonances by manipulating the classical dynamics, which can be realized by applying or withdrawing a properly designed local gate potential. Likewise, modulating the classical dynamics in a different way can enhance the resonance. This is of particular importance in the design of electronic switches that can control spin orientation of the electrons associated with the output current through weakening or enhancement of a Fano resonance, which are a key component in spintronics.

I. INTRODUCTION

The Fano formula was discovered [1] in 1961 to explain the sharply asymmetric profile experimentally observed in the absorption spectrum of Rydberg atoms [2]. A general form of the formula describing the resonance profile can be written as

$$\sigma = \frac{(\epsilon + q)^2}{1 + \epsilon^2}, \tag{1}$$

where σ is a measurable quantity such as the spectral intensity, the scattering cross section, or the conductance, etc., ϵ is the amount of the normalized energy deviated from the center of the resonance defined to be $\epsilon = 0$, and q is a parameter characterizing the degree of asymmetry of the resonance which is essential to experimental fitting of the resonance profile. Especially, for $q \neq 1$, the resonance profile is asymmetric because the quantity σ attains a maximum value at $\epsilon = 1/q$ and a minimum value at $\varepsilon = -q$. Fano resonances arise in scattering and transport processes and the validity of the formula has been established in a variety of two-dimensional (2D) electronic transport processes in mesoscopic systems [2–11], e.g., quantum dots [12, 13], and Anderson impurity systems [14]. In terms of quantum information, the Fano peaks correspond to the so-called "einselection" states [15–17].

For electronic transport through a quantum dot structure, the geometric shape of the dot (or scattering) region determines the particular type of classical dynamics, e.g., integrable, mixed (nonhyperbolic), or chaotic, and can affect the resonance profile [18]. In particular, for integrable or nonhyperbolic dynamics, there are stable periodic orbits in the dot region, in which a classical trajectory can be trapped indefinitely, i.e., with an infinite lifetime. In the corresponding quantum system, if the energy (or wave number) of the electron is such that the geometric distance along a stable periodic orbit is an integer multiple of the wavelength, constructive interference arises, leading to a quantum resonance at the particular energy value. Since the classical lifetime along a resonant stable periodic orbit is infinite, in principle the quantum resonance will be infinitely sharp which, however, cannot occur due to the effect of wave dispersion. Nonetheless, the resonance can be sharp. Because of the existence of various stable periodic orbits in the system with different orbital length, sharp resonances can occur at a discrete set of energy values [19], corresponding to the "einselection" states [7, 15, 17]. Due to the long dwelling time near a stable periodic orbit, associated with the resonance is degradation of wave coherence [20–22]. In contrast, for fully developed chaotic classical dynamics within the dot region, all periodic orbits are unstable, reducing significantly the quantum dwelling time and broadening the corresponding resonance profile. From a different perspective, the resonance peak and width, e.g., in an electronic transport system, can be exploited to detect and distinguish the corresponding classical dynamics [18] and to analyze wave coherence [20–22]. In fact, there were previous studies on characterizing or controlling quantum coherence through Fano resonance [3, 6, 23–25].

A vast majority of the previous work on Fano reso-

* huangl@lzu.edu.cn

nance in mesoscopic transport systems focused on electronic properties such as conductance, with spin largely ignored. In spintronics applications [26, 27], the spin degree of freedom of electrons plays a fundamental role. An issue of applied value is whether Fano resonances can arise in spin transport in 2D mesoscopic systems. In this regard, there were previous studies on spin-dependent Fano effect or resonance in electronic transport characteristics such as conductance [21, 23, 28–38]. In particular, the feasibility of performing single-spin readout in a quantum dot based on Fano resonance in conductance was studied [28], the interplay between Fano effect and Rashba spin-orbit interaction in an Aharanov-Bohm ring coupled with quantum dot systems was investigated [23, 29–31], and Fano-like backscattering leading to dips in the channel conductance was exploited for spin filtering [32]. In addition, spin filtering based on Fano resonances in open quantum dot systems was suggested [33]. It was also found that inelastic spin dependent electron scattering by a magnetic impurity and a spin dimer leading to spin flip can induce Fano resonances in the transport characteristics [34]. Spin interference and Fano effect in electron transport through mesoscopic ring side-coupled with a quantum dot [35] and spin-dependent Fano resonance induced by a conducting chiral helimagnet in a quasi-one-dimensional electron waveguide [36] were investigated. Spin filters and Fano antiresonances in conductance in a polymer device were studied using the nonequilibrium Green's function approach [37]. Spin-dependent Fano effect in a T-shaped double quantum dot was exploited to achieve perfect spin polarization [38]. We note that all previous efforts in this area concerned about the effect of spin on Fano resonances in conductance, i.e., spin-dependent Fano effect. Our focus is on *Fano resonances in quantities directly characterizing spin*, not on how different spin orientations affect Fano resonances in electronic properties such as conductance. A pertinent open question is whether a universal formula as Eq. (1) exists to characterize the Fano resonances in spin transport. To our knowledge, a systematic and mechanistic understanding of Fano resonances in physical quantities defined directly in terms of spin is lacking, and the goal of our paper is to develop such an understanding. Quantitatively, we analyze two fundamental quantities underlying spin transport: spin-resolved transmission and the spin polarization vector, and derive a Fano formula for both.

Concretely, we concentrate on spin transport through 2D quantum dot systems with Rashba spin-orbit interaction and preserved time-reversal symmetry. To be as general as possible, we choose the dot geometry such that the classical dynamics are of the mixed type [39–44], where the phase space contains both Kolmogorov-Arnold-Moser (KAM) tori and chaotic regions. Since the system is open, classically there is transient chaos or chaotic scattering of the nonhyperbolic nature [45]. Technically, our program to derive a Fano formula for spin transport is as follows. We first generalize the conventional Green's function to spin transport. We then exploit the Fisher-Lee relation [4, 24] to obtain the spin-resolved transmission matrix, which enables the spin polarization vector to be calculated. The end result of the calculation is a Fano-like formula in terms of the spin polarization vector. Finally, we study the effect of the geometric shape of the dot (or the nature of classical dynamics) on spin transport and articulate a spin control scheme. Prior to our work, a Fano-like formula for spin transport did not exist and, as we will demonstrate, our study has pertinent applied values in spintronics in terms of controlling/manipulating spin transport.

II. NONHYPERBOLIC QUANTUM DOT SYSTEM AND SPIN POLARIZATION VECTOR

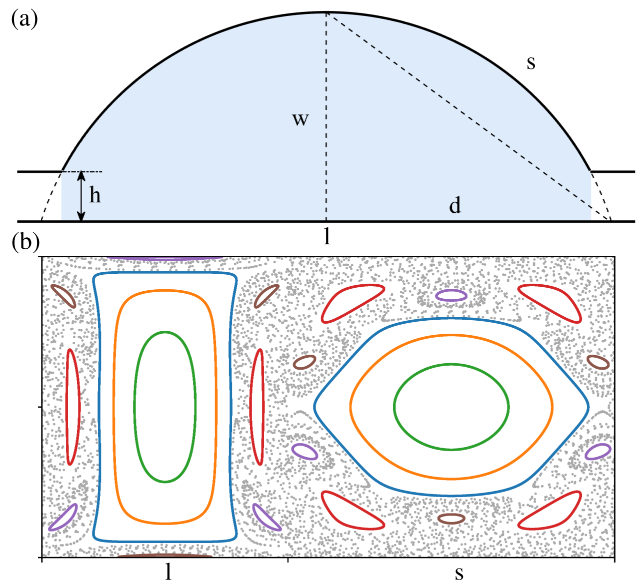

FIG. 1. *A schematic illustration of the bow shaped dot geometry and the phase space structure on the Poincaré surface of section.* (a) Geometry of the quantum dot: a bow shaped open cavity with two leads, one attached to the left and another to the right end. Geometric parameters are radius $R = 0.6\mu$m and cut width $w = 0.7R$. The height of the lead is $h = 0.2R$, which permits $N = 12$ transverse modes. (b) Poincaré surface of section of the corresponding closed cavity system in terms of the Birkhoff coordinates. The classical dynamics are mixed or nonhyperbolic.

We study quantum dot systems with a bow-shaped type of scattering region, as shown in Fig. 1(a). In the mesoscopic regime, representative parameter values are: radius $R = 0.6\mu$m and the cut width $w = 0.7R$ (so the chord length is $l = 2d = 2\sqrt{R^2 - w^2}$), and s is the arc length of the upper circular section. We attach two identical leads of height $h = 0.2R$: one to the left and another to the right end of the open cavity. In the lead, there are $N = 12$ transverse modes at most. Rashba spin-orbit interaction exists in the shaded region [46] with an electrical field $\boldsymbol{E}$ applied perpendicular to the cavity plane. Figure 1(b) illustrates the structure of the classical phase space on the Poincaré surface of section in terms of the Birkhoff coordinates [47] of the corresponding closed billiard system. There is a mixture of KAM tori and chaotic sea [48], signifying nonhyperbolic dynamics [45].

An effective approach to modulating spin transport is to create a large KAM island in the classical phase space so as to generate strong quantum localized states that lead to sharp Fano resonances, which can be broken by tuning an externally controllable parameter. Here, we test the scenario to generate a circular forbidden region in the quantum dot structure by applying a locally repulsive potential and demonstrate that this configuration is effective at harnessing spin transport. However, we choose to study this model only for simplicity and it is not special in the sense that there are many alternative configurations that can be exploited for controlling spin transport.

The Hamiltonian of the 2D spin transport system is

$$\hat{\mathcal{H}} = \frac{\hbar^2}{2m}(\hat{k}_x^2 + \hat{k}_y^2)\sigma_0 + \alpha(\hat{\sigma}_x\hat{k}_y - \hat{\sigma}_y\hat{k}_x) \ . \tag{2}$$

where σ_0 is the 2×2 identity matrix, $\hat{\sigma}_x$ and $\hat{\sigma}_y$ are Pauli matrices. To solve the Schrödinger equation, we discretize the cavity into 3888 lattice cells. We set the energy in units of $t_0 = \hbar^2/(2ma^2)$, where a is the lattice constant, and fix the strength of spin-orbit coupling to be $\alpha = 0.1t_0$. Consider an electron entering the quantum dot system from the left lead. We denote the state in the lead as $|n\rangle$ and, to be specific, we assume that the electron is in the spin-↑ state. With respect to the dot region, the incoming and the outgoing states, respectively, can be written as [49–51]

$$|\text{in}\rangle = |n\rangle \otimes |\sigma = \uparrow\rangle \ , \tag{3}$$

$$|\text{out}\rangle = \sum_{n',\sigma'} t_{n'n,\sigma'\uparrow} |n'\rangle \otimes |\sigma'\rangle \ . \tag{4}$$

where $t_{n'n,\sigma'\uparrow}$ is the transition amplitude from the incoming state $|n\rangle$ with spin-↑ to the outgoing state $|n'\rangle$ with spin-σ. The spin density matrix $\hat{\rho}_s$ carries complete information about the spin state over the orbital degree of freedom. Let $\hat{\rho}$ be the density matrix characterizing the full state of the system. We can write [50, 51] $\hat{\rho}_s = \text{Tr}_{orbit}\,\hat{\rho}$, which can be expressed in terms of the spin polarization vector defined as the quantum average of the Pauli spin operator vector [49–51]:

$$\mathbf{P} = \langle\psi|\hat{\boldsymbol{\sigma}}|\psi\rangle, \tag{5}$$

which contains the information about spin-orbit entanglement or spin decoherence [50, 52, 53]. The spin density matrix can then be written as [50, 51, 54],

$$\begin{aligned}\hat{\rho}_s &= \frac{1}{\sum_\sigma \text{Tr}(\boldsymbol{t}_{\sigma\uparrow}\boldsymbol{t}_{\sigma\uparrow}^\dagger)} \begin{pmatrix} \text{Tr}(\boldsymbol{t}_{\uparrow\uparrow}\boldsymbol{t}_{\uparrow\uparrow}^\dagger) & \text{Tr}(\boldsymbol{t}_{\downarrow\uparrow}\boldsymbol{t}_{\uparrow\uparrow}^\dagger) \\ \text{Tr}(\boldsymbol{t}_{\uparrow\uparrow}\boldsymbol{t}_{\downarrow\uparrow}^\dagger) & \text{Tr}(\boldsymbol{t}_{\downarrow\uparrow}\boldsymbol{t}_{\downarrow\uparrow}^\dagger) \end{pmatrix} \\ &= \frac{1}{2}\begin{pmatrix} 1+\text{P}_z & \text{P}_x - i\text{P}_y \\ \text{P}_x + i\text{P}_y & 1-\text{P}_z \end{pmatrix}. \end{aligned} \tag{6}$$

where $\boldsymbol{t}_{\sigma\uparrow}$ ($\sigma =\uparrow,\downarrow$) is the spin resolved transmission matrix for incoming electrons with spin-↑ and outgoing electrons with spin-σ. The three components of the polarization vector $\mathbf{P}$ are [18, 51]

$$\begin{aligned} \text{P}_x &= \frac{2\,\text{Re}[\text{Tr}(\boldsymbol{t}_{\downarrow\uparrow}\boldsymbol{t}_{\uparrow\uparrow}^\dagger)]}{\text{Tr}(\boldsymbol{t}_{\uparrow\uparrow}\boldsymbol{t}_{\uparrow\uparrow}^\dagger) + \text{Tr}(\boldsymbol{t}_{\downarrow\uparrow}\boldsymbol{t}_{\downarrow\uparrow}^\dagger)}, \\ \text{P}_y &= \frac{2\,\text{Im}[\text{Tr}(\boldsymbol{t}_{\downarrow\uparrow}\boldsymbol{t}_{\uparrow\uparrow}^\dagger)]}{\text{Tr}(\boldsymbol{t}_{\uparrow\uparrow}\boldsymbol{t}_{\uparrow\uparrow}^\dagger) + \text{Tr}(\boldsymbol{t}_{\downarrow\uparrow}\boldsymbol{t}_{\downarrow\uparrow}^\dagger)}, \\ \text{P}_z &= \frac{\text{Tr}(\boldsymbol{t}_{\uparrow\uparrow}\boldsymbol{t}_{\uparrow\uparrow}^\dagger) - \text{Tr}(\boldsymbol{t}_{\downarrow\uparrow}\boldsymbol{t}_{\downarrow\uparrow}^\dagger)}{\text{Tr}(\boldsymbol{t}_{\uparrow\uparrow}\boldsymbol{t}_{\uparrow\uparrow}^\dagger) + \text{Tr}(\boldsymbol{t}_{\downarrow\uparrow}\boldsymbol{t}_{\downarrow\uparrow}^\dagger)}. \end{aligned} \tag{7}$$

Equation (7) indicates that the polarization vector can be expressed solely in terms of the spin-resolved matrix governing the transmission properties. Figure 2 shows the spin-resolved transmission and spin polarization vector versus Fermi energy. An example of Fano resonance in spin-resolved transmission is shown in Fig. 3. Several examples of Fano resonance in the spin polarization vector is shown in Fig. 4.

In the following, we will show analytically that the spin-resolved transmission and the spin polarization vector $\mathbf{P}$ possess Fano resonances characterizable by a formula similar to Eq. (1) for electronic conductance.

III. FANO RESONANCES IN SPIN TRANSPORT AND FANO FORMULA

A. Green's function

For 2D mesoscopic electronic transport systems, there were previous studies of Fano resonances [2, 3, 5–7] based on the Green's function, where the spin degree of freedom was ignored. Here we generalize the approach of Green's function to spin transport systems with Rashba spin-orbit interaction.

1. *Spin-resolved Green's function*

For a typical 2D transport system, the Hamiltonian (2) can be decomposed into two parts: $\hat{H}_c = \hat{H}_o + \hat{H}_{so}$, where $\hat{H}_o$ is the original spinless Hamiltonian while $\hat{H}_{so}$ is the Hamiltonian for the spin-orbit interaction. The spin-resolved self energy in the leads can be expressed as $\Sigma^R = \Sigma_0^R\sigma_0$ under the assumption that the self energies of the spin-↑ and spin-↓ states are equal. The effective Hamiltonian of the whole system, taking into account the lead self energies, can be written as $\hat{H}_s = \hat{H}_c + \Sigma^R$. The Hamiltonian preserves the time reversal symmetry because the time-reversal operator [55] $\hat{\Theta}$ of the single particle spin-1/2 system commutes with the Hamiltonian: $[\hat{\Theta}, \hat{H}_s] = 0$. The time reversal symmetry leads to *Kramers degeneracy*: if state $|n\rangle$ is an eigenstate of the system $\hat{H}$, then its time reversed state $|\hat{\Theta}n\rangle$ is also an

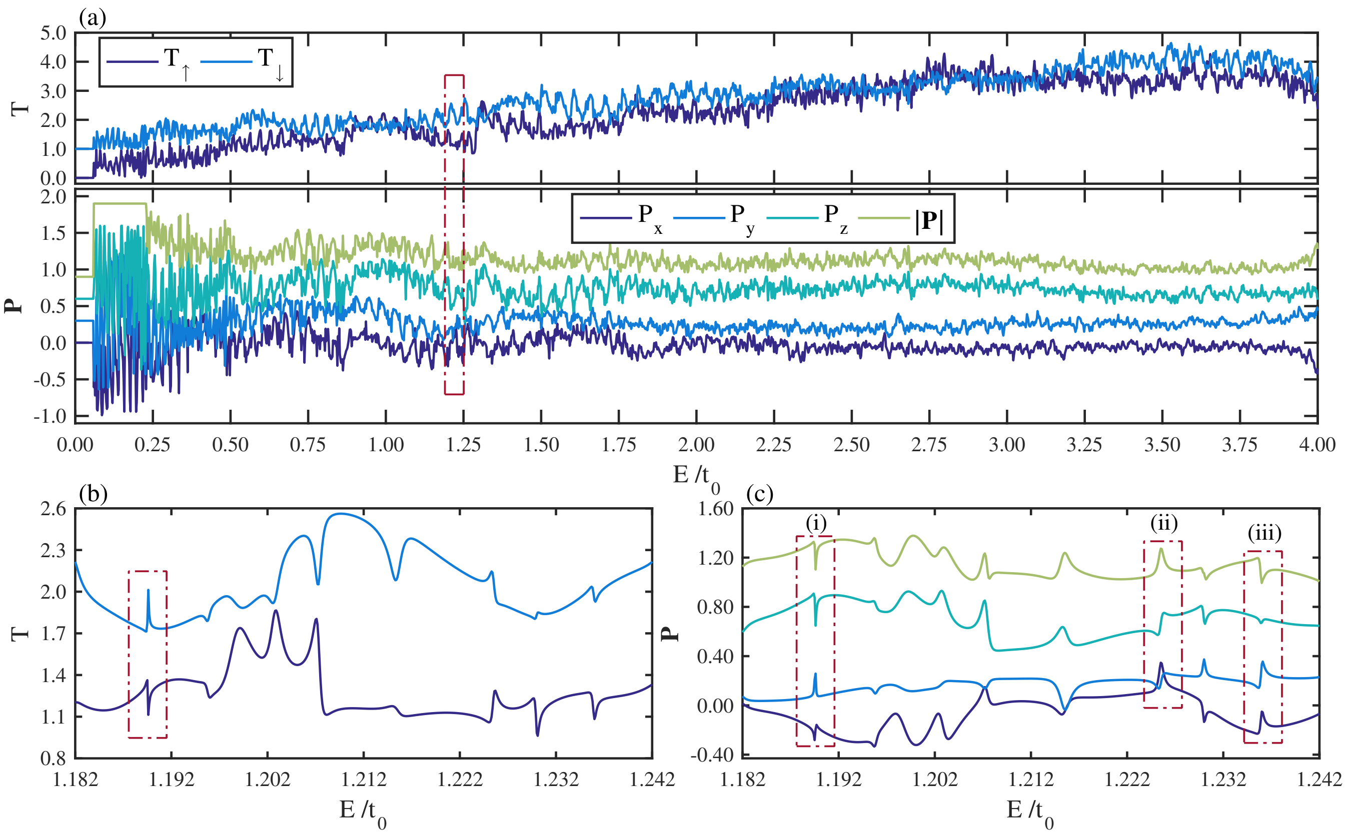

FIG. 2. *Spin-resolved transmission and spin polarization vector versus Fermi energy.* (a) Variations of the spin-resolved transmission T_σ and the spin polarization vector $\mathbf{P}$ versus E (in units of the hopping energy t_0) in the entire energy interval considered. (b,c) Magnification of the behavior of T_σ and the three components of $\mathbf{P}$ as well as its magnitude, respectively, in an arbitrarily chosen energy interval enclosed by the dark red dash-dotted box in (a). The dark red dash-dotted box covering a resonance peak in (b) is fitted by the theoretical prediction in Fig. 3. The other three dark red dash-dotted boxes labeled as (i), (ii) and (iii) covering three peaks in (c) are fitted by the theoretical results in Fig. 4. The curves from bottom up in (b) correspond to $T_\uparrow$ and $T_\downarrow$, while those in (c) are for P_x, P_y, P_z and $|\mathbf{P}|$. For visualization, a vertical shift has been applied in the amount of 1.0 for $T_\downarrow$ and 0.3, 0.6, 0.9 for P_y, P_z and $|\mathbf{P}|$, respectively.

eigenstate with the same energy, where $\langle n|\hat{\Theta}n\rangle = 0$ and the degree of degeneracy is $2j+1$ with j being the angular momentum quantum number of the system [54, 55].

Because of the inclusion of the self energies, the system described by the Hamiltonian $\hat{H}_s$ is non-Hermitian with complex eigenvalues and non-identical left and right eigenstates. The eigenequations distinguishing the left and right eigenstates are

$$\hat{H}_s|\psi_{\alpha,\mu}\rangle = \varepsilon_\alpha|\psi_{\alpha,\mu}\rangle, \tag{8}$$

$$\langle\Phi_{\alpha,\mu}|\hat{H}_s = \langle\Phi_{\alpha,\mu}|\varepsilon_\alpha. \tag{9}$$

where $\mu = 1, 2$ denotes the two Kramer's degenerate eigenstates. The eigenstates $|\psi_{\alpha,\mu}\rangle$ and $|\Phi_{\alpha,\mu}\rangle$ constitute a bi-orthonormal basis set [4] under the renormalization

$$|\Phi_{\alpha,\mu}\rangle = |\varphi_{\alpha,\mu}\rangle/\langle\varphi_{\alpha,\mu}|\psi_{\beta,\nu}\rangle,$$

where the left vector $\langle\varphi_{\alpha,\mu}|$ satisfies $\langle\varphi_{\alpha,\mu}|\hat{H}_s = \langle\varphi_{\alpha,\mu}|\varepsilon_\alpha$.

The bi-orthonormal conditions are

$$\langle\Phi_{\alpha,\mu}|\psi_{\beta,\nu}\rangle = \langle\psi_{\alpha,\mu}|\Phi_{\beta,\nu}\rangle = \delta_{\alpha\beta}\delta_{\mu\nu}, \tag{10}$$

$$\sum_\mu\sum_\alpha|\psi_{\alpha,\mu}\rangle\langle\Phi_{\alpha,\mu}| = \sum_\mu\sum_\alpha|\Phi_{\alpha,\mu}\rangle\langle\psi_{\alpha,\mu}| = 1. \tag{11}$$

For an isolated dot system without any self energy, the Hamiltonian is Hermitian. In this case, we have

$$\hat{H}_c|\psi_{\alpha,\mu}\rangle = \varepsilon_{\alpha,0}|\psi_{\alpha,\mu}\rangle, \tag{12}$$

with the orthonormal condition:

$$\langle\psi_{\alpha,\mu}|\psi_{\beta,\nu}\rangle = \delta_{\alpha\beta}\delta_{\mu\nu}. \tag{13}$$

Making use of Eq. (10), we can derive the Green's func-

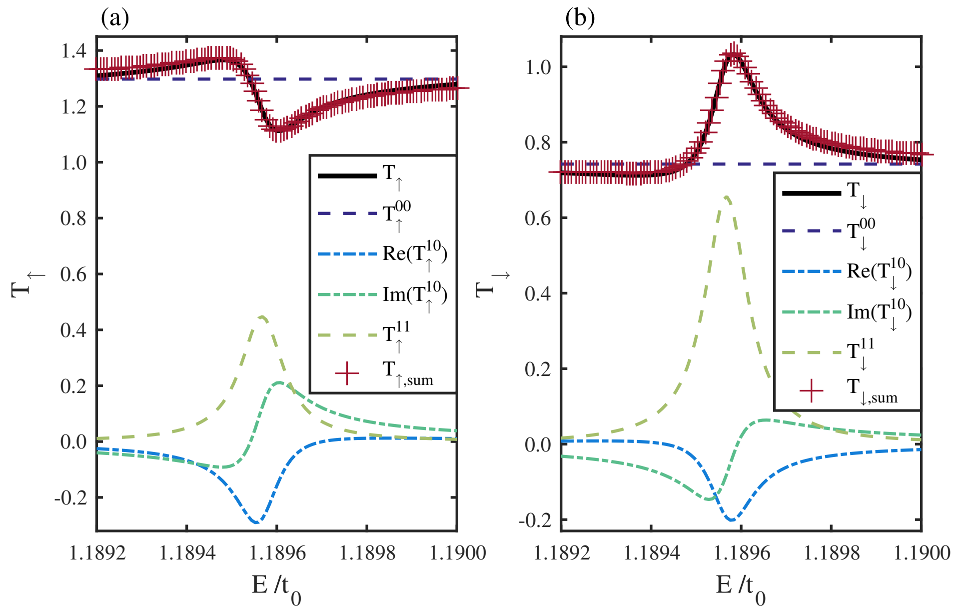

FIG. 3. *Illustration of a Fano resonance in spin-resolved transmission.* A comparison of (a) $T_\uparrow$ and (b) $T_\downarrow$ for the peak covered by the dash-dotted box in Fig. 2(b) with Eq. (26). The dark red pluses are theoretical prediction and the black curves (mostly beneath the dark red pluses) represent numerical results.

tion for the central dot region as

$$
\begin{aligned}
G^R(\boldsymbol{r},\boldsymbol{r}') &= \langle \boldsymbol{r}|\frac{1}{E-\hat{H}_s}|\boldsymbol{r}'\rangle \\
&= \sum_{\alpha,\mu}\sum_{\beta,\nu}\langle \boldsymbol{r}|\psi_{\alpha,\mu}\rangle\langle\Phi_{\alpha,\mu}|\frac{1}{E-\hat{H}_s}|\psi_{\beta,\nu}\rangle\langle\Phi_{\beta,\nu}|\boldsymbol{r}'\rangle \\
&= \sum_{\alpha,\mu}\sum_{\beta,\nu}\psi_{\alpha,\mu}(\boldsymbol{r})\frac{1}{E-\varepsilon_\beta}\delta_{\alpha\beta}\delta_{\mu\nu}\Phi^\dagger_{\beta,\nu}(\boldsymbol{r}') \\
&= \sum_{\mu}\sum_{\alpha}\frac{\psi_{\alpha,\mu}(\boldsymbol{r})\Phi^\dagger_{\alpha,\mu}(\boldsymbol{r}')}{E-\varepsilon_\alpha} \\
&= \begin{pmatrix} G^R_{\uparrow\uparrow}(\boldsymbol{r},\boldsymbol{r}') & G^R_{\uparrow\downarrow}(\boldsymbol{r},\boldsymbol{r}') \\ G^R_{\downarrow\uparrow}(\boldsymbol{r},\boldsymbol{r}') & G^R_{\downarrow\downarrow}(\boldsymbol{r},\boldsymbol{r}') \end{pmatrix}. \qquad (14)
\end{aligned}
$$

The spin-resolved Green's function can be written as

$$
G^R_{\sigma\sigma'}(\boldsymbol{r},\boldsymbol{r}') = \sum_{\mu=1,2}\sum_{\alpha}\frac{\psi^\sigma_{\alpha,\mu}(\boldsymbol{r})\Phi^{\sigma'\dagger}_{\alpha,\mu}(\boldsymbol{r}')}{E-\varepsilon_\alpha}, \quad \sigma,\sigma' = \uparrow,\downarrow . \qquad (15)
$$

Because of the spin-orbit interaction, the eigenfunctions are spinors:

$$
\Phi_{\alpha,\mu}(\boldsymbol{r}') = \begin{pmatrix} \Phi^\uparrow_{\alpha,\mu}(\boldsymbol{r}') \\ \Phi^\downarrow_{\alpha,\mu}(\boldsymbol{r}') \end{pmatrix}, \qquad
\psi_{\alpha,\mu}(\boldsymbol{r}) = \begin{pmatrix} \psi^\uparrow_{\alpha,\mu}(\boldsymbol{r}) \\ \psi^\downarrow_{\alpha,\mu}(\boldsymbol{r}) \end{pmatrix}.
$$

Treating the self energy Σ^R as a perturbation [4, 11], we can use the perturbation theory to expand the eigenenergies and the eigenstates as

$$
\varepsilon_\alpha = \varepsilon_{0,\alpha} - \delta_\alpha - i\gamma_\alpha , \qquad (16)
$$

$$
|\psi_{\alpha,\mu}\rangle = |\psi_{0\alpha,\mu}\rangle - |\psi_{r\alpha,\mu}\rangle - i|\psi_{i\alpha,\mu}\rangle. \qquad (17)
$$

Substituting Eqs. (16) and (17) into Eq. (9), we get

$$
\left(\hat{H}_c + \Sigma^R\right)(|\psi_{0\alpha,\mu}\rangle - |\psi_{r\alpha,\mu}\rangle - i|\psi_{i\alpha,\mu}\rangle) = (\varepsilon_{0,\alpha} - \delta_\alpha - i\gamma_\alpha)(|\psi_{0\alpha,\mu}\rangle - |\psi_{r\alpha,\mu}\rangle - i|\psi_{i\alpha,\mu}\rangle).
$$

Substituting Eq. (12) into the above, neglecting second-order terms on both sides, and left-multiplying both sides with $\langle\psi_{0\alpha,\mu}|$, we obtain [4, 11]

$$
\begin{aligned}
\delta_\alpha + i\gamma_\alpha &\simeq -\sum_{\mu}\langle\psi_{0\alpha,\mu}|\Sigma^R|\psi_{0\alpha,\mu}\rangle \\
&= -\sum_{\mu,\sigma}\langle\psi^\sigma_{0\alpha,\mu}|\Sigma^R_0|\psi^\sigma_{0\alpha,\mu}\rangle, \qquad (18)
\end{aligned}
$$

where the spin components of the eigenstates and the relation $\Sigma^R = \Sigma^R_0\sigma_0$ have been used. Equation (16) can be rewritten as

$$
\varepsilon_\alpha \simeq \varepsilon_{\alpha,0} - \sum_{\mu,\sigma}\langle\psi^\sigma_{0\alpha,\mu}|\Sigma^R_0|\psi^\sigma_{0\alpha,\mu}\rangle. \qquad (19)
$$

The resonance width γ_α can be obtained from Eq. (18) as [4, 11]

$$
\begin{aligned}
\gamma_\alpha &= -\mathrm{Im}\left(\sum_{\mu,\sigma}\langle\psi^\sigma_{0\alpha,\mu}|\Sigma^R_0|\psi^\sigma_{0\alpha,\mu}\rangle\right) \\
&= \sum_{\mu,\sigma}\langle\psi^\sigma_{0\alpha,\mu}|\left[-\mathrm{Im}(\Sigma^R_0)\right]|\psi^\sigma_{0\alpha,\mu}\rangle. \qquad (20)
\end{aligned}
$$

This expression will be validated by comparing it with the exact value in Eq. (16) (c.f., Fig. 5).

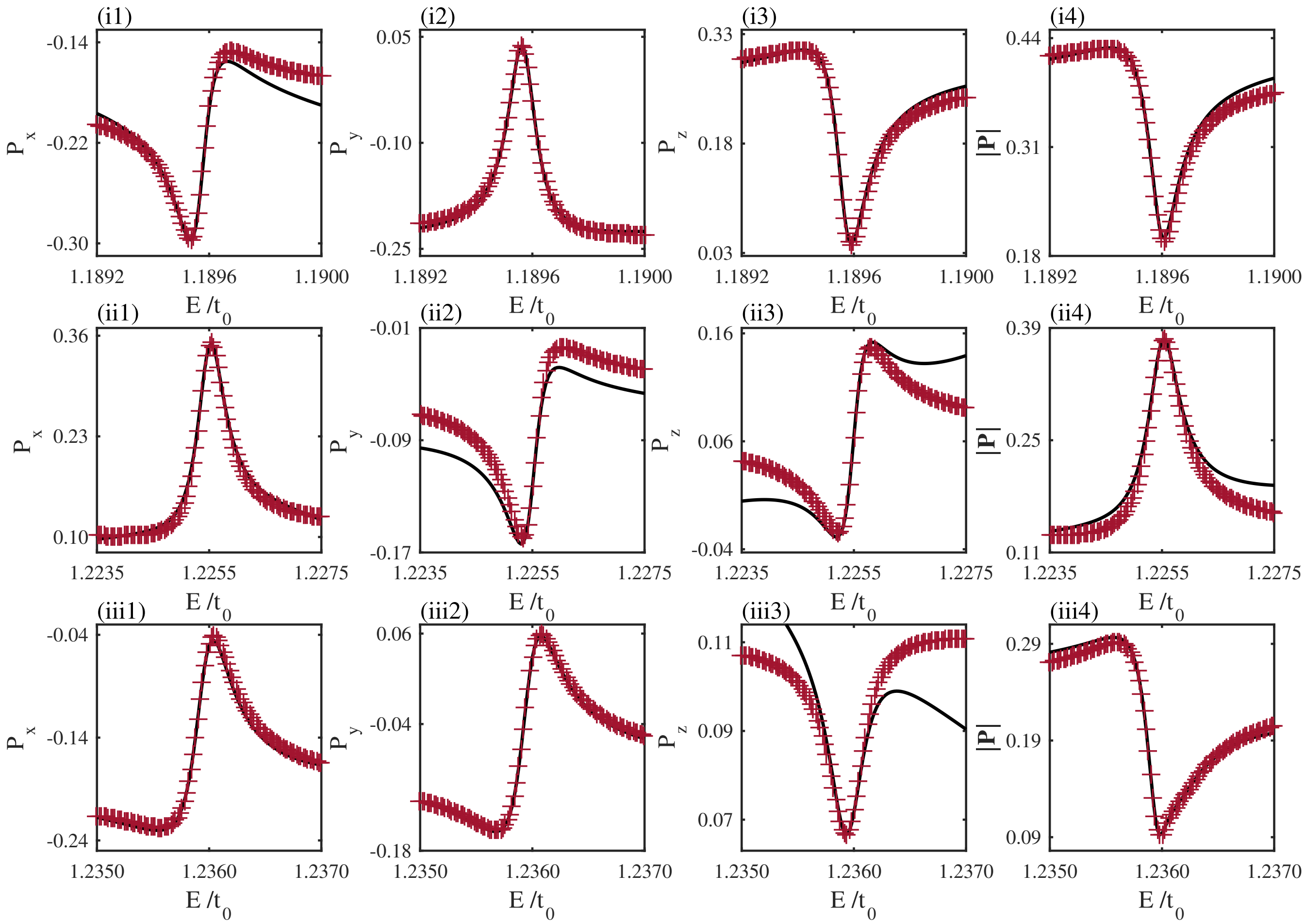

FIG. 4. *Illustration of Fano resonances in spin polarization vector.* For **P** in Eq. (29), panels (i-iii) in each column correspond to the three peaks covered by the dashed black box in Fig. 2(c), and panels (1-4) of each row show the numerical (black curve) and theoretical (plus symbols) results for P_x, P_y, P_z, and $|\mathbf{P}|$, respectively.

2. *Fisher-Lee relation*

The Fisher-Lee relation connects the S-matrix with the Green's function [4, 24]. For a two-terminal system with left and right leads, the spin-resolved Fisher-Lee relation can be expressed as

$$
\begin{aligned}
s_{nm}^{\sigma\sigma'} &= -\delta_{mn}\delta^{\sigma\sigma'} + i\hbar\sqrt{v_m v_n}\int \chi_n(y_q) G^R_{\sigma\sigma'}\chi_m(y_p) dy_p dy_q \\
&= -\delta_{mn}\delta^{\sigma\sigma'} + i\sqrt{\hbar v_n}\cdot R_{nm}^{\sigma\sigma'}\cdot\sqrt{\hbar v_m}\ , \qquad (21)
\end{aligned}
$$

where m and n belong to lead p and q, respectively; and

$$
\begin{aligned}
R_{nm}^{\sigma\sigma'} &= \sum_{\mu=1,2}\sum_{\alpha}\frac{\psi^{\sigma}_{\alpha n,\mu}(x_q)\Phi^{\sigma'\dagger}_{\alpha m,\mu}(x_p)}{E-\varepsilon_\alpha}, \\
\psi^{\sigma}_{\alpha n,\mu}(x_q) &= \int \chi_n(y_q)\psi^{\sigma}_{\alpha n,\mu}(x_q, y_q) dy_q, \\
\Phi_{\alpha m,\mu}(x_p) &= \int \chi_m(y_p)\Phi^{\sigma}_{\alpha m,\mu}(x_p, y_p) dy_p, \\
V_{p/q} &= \mathrm{diag}\{\hbar v_1, \hbar v_2, \cdots, \hbar v_{N_{p/q}}\}.
\end{aligned}
$$

For p and q corresponding to different leads, $s_{nm}^{\sigma\sigma'}$ is a transmission matrix, while for $p = q =$ left lead, it is a reflection matrix. The spin-resolved transmission matrix can be expressed in the following concise form:

$$
\boldsymbol{t}_{\sigma\sigma'} = i\sqrt{V_q}\cdot R^{\sigma\sigma'}\cdot\sqrt{V_p}. \qquad (22)
$$

For convenience, we let p and q specify the left and right lead, respectively. With the spin-resolved transmission matrix, we can calculate the spin-resolved transmission and the spin polarization vector in Eq. (7).

B. Fano resonances in spin-resolved transmission and spin polarization vector

We derive Fano resonance formulas for spin-resolved transmission and the spin polarization vector **P**. Say we select E_0 as the energy of interest. If E_0 approaches an eigenenergy of the closed dot system, a pole will arise in $R_{\sigma\sigma',nm}$, corresponding to a specific state labeled by, e.g., α. We can then separate state α from the sum in $R_{\sigma\sigma',nm}$ to get two terms: one slowly varying (with energy) and another rapidly changing term, where the former acts effectively as the background while the latter varies rapidly in the small energy interval containing state α [11, 20, 22, 24]. Specifically, we have

$$R^{\sigma\sigma'}_{nm} = R^{0,\sigma\sigma'}_{nm} + R^{1,\sigma\sigma'}_{nm} = \sum_{\mu=1,2}\sum_{\beta\neq\alpha} \frac{\psi^{\sigma}_{\beta n,\mu}(x_r)\Phi^{\sigma'\dagger}_{\beta m,\mu}(x_l)}{E-\varepsilon_\beta} + \sum_{\mu=1,2} \frac{\psi^{\sigma}_{\alpha n,\mu}(x_r)\Phi^{\sigma'\dagger}_{\alpha m,\mu}(x_l)}{E-\varepsilon_\alpha}. \tag{23}$$

The spin-resolved transmission matrix in Eq. (22) can be rewritten as the sum of the slowly varying background term and the fast changing resonance term. For incoming spin-↑ state, we have,

$$\boldsymbol{t}_{\sigma\uparrow} = \boldsymbol{t}^0_{\sigma\uparrow} + \boldsymbol{t}^1_{\sigma\uparrow}, \tag{24}$$

where the first and second terms represent the slow and fast terms, respectively. The spin-resolved transmission

$$\mathrm{T}_\sigma = \mathrm{Tr}[\boldsymbol{t}_{\sigma\uparrow}\boldsymbol{t}^\dagger_{\sigma\uparrow}]$$

can be obtained, from which the Fano resonance formulas for T_σ and $\mathbf{P}$ can be derived.

1. Fano formula for spin-resolved transmission T_σ

Substituting Eq. (24) into the definition of the spin-resolved transmission T_σ, we have

$$\begin{aligned}\mathrm{T}_\sigma &= \mathrm{Tr}[\boldsymbol{t}_{\sigma\uparrow}\boldsymbol{t}^\dagger_{\sigma\uparrow}] \\ &= \mathrm{Tr}[(\boldsymbol{t}^0_{\sigma\uparrow}+\boldsymbol{t}^1_{\sigma\uparrow})(\boldsymbol{t}^0_{\sigma\uparrow}+\boldsymbol{t}^1_{\sigma\uparrow})^\dagger] \\ &= \mathrm{Tr}[\boldsymbol{t}^0_{\sigma\uparrow}\boldsymbol{t}^{0\dagger}_{\sigma\uparrow}] + \mathrm{Tr}[\boldsymbol{t}^0_{\sigma\uparrow}\boldsymbol{t}^{1\dagger}_{\sigma\uparrow}] + \mathrm{Tr}[\boldsymbol{t}^1_{\sigma\uparrow}\boldsymbol{t}^{0\dagger}_{\sigma\uparrow}] + \mathrm{Tr}[\boldsymbol{t}^1_{\sigma\uparrow}\boldsymbol{t}^{1\dagger}_{\sigma\uparrow}] \\ &= \mathrm{T}^{00}_\sigma + \mathrm{T}^{01}_\sigma + \mathrm{T}^{10}_\sigma + \mathrm{T}^{11}_\sigma,\end{aligned}$$

where $\mathrm{T}^{00}_\sigma(E) \simeq \mathrm{T}^{00}_\sigma(E_0)$ is approximately a constant [11] in the small energy interval containing the specific energy value E_α. Letting $\epsilon \equiv (E-E_\alpha)/\gamma_\alpha$ and $\epsilon_0 \equiv (E_0 - E_\alpha)/\gamma_\alpha$, we have

$$\begin{aligned}\mathrm{T}^{01}_\sigma(E) &= \mathrm{T}^{01}_\sigma(E_0)\frac{E_0-E_\alpha-i\gamma_\alpha}{E-E_\alpha-i\gamma_\alpha} \\ &= \mathrm{T}^{01}_\sigma(E_0)\frac{\epsilon_0-i}{\epsilon-i}, \\ \mathrm{T}^{10}_\sigma(E) &= \mathrm{T}^{10}_\sigma(E_0)\frac{E_0-E_\alpha+i\gamma_\alpha}{E-E_\alpha+i\gamma_\alpha} \\ &= \mathrm{T}^{10}_\sigma(E_0)\frac{\epsilon_0+i}{\epsilon+i}, \\ \mathrm{T}^{11}_\sigma(E) &= \mathrm{T}^{11}_\sigma(E_0)\frac{(E_0-E_\alpha)^2+\gamma_\alpha^2}{(E-E_\alpha)^2+\gamma_\alpha^2} \\ &= \mathrm{T}^{11}_\sigma(E_0)\frac{\epsilon_0^2+1}{\epsilon^2+1}.\end{aligned}$$

For $E_0 = E_\alpha$, we have $\epsilon_0 = 0$. Denoting

$$\Delta\mathrm{T}_\sigma = \mathrm{T}^{01}_\sigma(E_0) + \mathrm{T}^{10}_\sigma(E_0) + \mathrm{T}^{11}_\sigma(E_0), \tag{25a}$$

$$q_\sigma = \frac{i}{2}\frac{\mathrm{T}^{10}_\sigma(E_0) - \mathrm{T}^{01}_\sigma(E_0)}{\Delta\mathrm{T}_\sigma(E_0)}, \tag{25b}$$

we obtain an explicit expression for $\mathrm{T}_{\sigma,sum}$:

$$\begin{aligned}\mathrm{T}_{\sigma,sum} &= \mathrm{T}^{00}_\sigma + \mathrm{T}^{01}_\sigma + \mathrm{T}^{10}_\sigma + \mathrm{T}^{11}_\sigma \\ &= \mathrm{T}^{00}_\sigma + \frac{1+2q_\sigma\epsilon}{1+\epsilon^2}\Delta\mathrm{T}_\sigma \\ &= |t^{bg}_\sigma|^2\frac{|\epsilon+q'_\sigma|^2}{\epsilon^2+1}\end{aligned} \tag{26}$$

with the relation

$$\begin{aligned}|t^{bg}_\sigma|^2 &= \mathrm{T}^{00}_\sigma\ , \\ \mathrm{Re}(q'_\sigma) &= \Delta\mathrm{T}_\sigma q_\sigma/\mathrm{T}^{00}_\sigma\ , \\ \mathrm{Im}(q'_\sigma) &= \sqrt{1+\Delta\mathrm{T}_\sigma/\mathrm{T}^{00}_\sigma - q_\sigma^2(\Delta\mathrm{T}_\sigma/\mathrm{T}^{00}_\sigma)^2}.\end{aligned}$$

Equation (26) presents the Fano resonance form [11, 20] with the complex profile parameter q'_σ that depends on q_σ, T^{00}_σ, and $\Delta\mathrm{T}_\sigma$. Fano resonances in the spin-resolved transmission can thus be characterized by a formula similar in form to that for the spinless conductance in Refs. [24,11].

2. Fano resonance formula for spin polarization vector

The components of $\mathbf{P}$ in Eq. (7) depend on T_σ and the cross term of the spin density matrix denoted as

$$\mathrm{T}_c = \mathrm{Tr}(\boldsymbol{t}_{\downarrow\uparrow}\boldsymbol{t}^\dagger_{\uparrow\uparrow}).$$

We check and find that T_c exhibits Fano resonances that can be described by the same formula as for T_σ. Particularly, we have

$$\begin{aligned}\mathrm{T}_{c,sum} &= \mathrm{T}^{00}_c + \mathrm{T}^{01}_c + \mathrm{T}^{10}_c + \mathrm{T}^{11}_c \\ &= \mathrm{T}^{00}_c + \frac{1+2q_c\epsilon}{1+\epsilon^2}\Delta\mathrm{T}_c \\ &= |t^{bg}_c|^2\frac{|\epsilon+q'_c|^2}{\epsilon^2+1},\end{aligned} \tag{27}$$

where the coefficients are given by

$$\Delta\mathrm{T}_c = \mathrm{T}^{01}_c(E_0) + \mathrm{T}^{10}_c(E_0) + \mathrm{T}^{11}_c(E_0)\ , \tag{28a}$$

$$q_c = \frac{i}{2}\frac{\mathrm{T}^{10}_c(E_0) - \mathrm{T}^{01}_c(E_0)}{\Delta\mathrm{T}_c(E_0)}, \tag{28b}$$

with the relations

$$\begin{aligned}|t^{bg}_c|^2 &= \mathrm{T}^{00}_c\ , \\ \mathrm{Re}(q'_c) &= \Delta\mathrm{T}_c q_c/\mathrm{T}^{00}_c\ , \\ \mathrm{Im}(q'_c) &= \sqrt{1+\Delta\mathrm{T}_c/\mathrm{T}^{00}_c - q_c^2(\Delta\mathrm{T}_c/\mathrm{T}^{00}_c)^2}.\end{aligned}$$

To obtain a Fano formula for the spin polarization vector, we need to substitute the quantity T_σ in Eq. (26) and T_c in Eq. (27) into Eq. (7). Note that the components of

$\mathbf{P}$ are fractions with both numerator and denominator expressed by the trace of the spin-resolved transmission matrix. After some algebraic manipulations, we obtain

$$\begin{aligned}\mathrm{P}_i &= \mathrm{P}_{i,0} + \frac{1+2Q\Xi}{1+\Xi^2}\Delta\mathrm{P}_i \\ &= |p_i^{bg}|^2 \frac{|Q'+\Xi|^2}{1+\Xi^2},\end{aligned} \tag{29}$$

where $i = x, y, z$ denote the three components of the spin polarization vector and the renormalized energy is

$$\begin{aligned}\Xi &= \sqrt{S}\left[\epsilon + \frac{\sum_\sigma (q_\sigma \Delta\mathrm{T}_\sigma)}{\sum_\sigma \mathrm{T}_\sigma^{00}}\right] \\ &= \frac{E - \left[\mathrm{Re}(\varepsilon_\alpha) - \gamma_\alpha \frac{\sum_\sigma (q_\sigma \Delta\mathrm{T}_\sigma)}{\sum_\sigma \mathrm{T}_\sigma^{00}}\right]}{\gamma_\alpha/\sqrt{S}}.\end{aligned} \tag{30}$$

With the coefficients in Eq. (29), we can combine Eqs. (25a) and (28a) to get

$$\begin{aligned}\mathrm{P}_0 &= \frac{\hat{\mathrm{O}}\mathrm{T}_s^{00}}{\sum_\sigma \mathrm{T}_\sigma^{00}}\ , \\ \Delta\mathrm{P} &= \frac{\hat{\mathrm{O}}\Delta\mathrm{T}_s - \mathrm{P}_0\sum_\sigma \Delta\mathrm{T}_\sigma - 2[\hat{\mathrm{O}}(q_s\Delta\mathrm{T}_s) - \mathrm{P}_0\sum_\sigma(q_\sigma\Delta\mathrm{T}_\sigma)]\frac{\sum_\sigma(q_\sigma\Delta\mathrm{T}_\sigma)}{\sum_\sigma \mathrm{T}_\sigma^{00}}}{(\sum_\sigma \mathrm{T}_\sigma^{00} + \sum_\sigma \Delta\mathrm{T}_\sigma) - \frac{[\sum_\sigma(q_\sigma\Delta\mathrm{T}_\sigma)]^2}{\sum_\sigma \mathrm{T}_\sigma^{00}}}, \\ Q &= \frac{1}{\sqrt{S}}\frac{\hat{\mathrm{O}}(q_s\Delta\mathrm{T}_s) - \mathrm{P}_0\sum_\sigma(q_\sigma\Delta\mathrm{T}_\sigma)}{\hat{\mathrm{O}}\Delta\mathrm{T}_s - \mathrm{P}_0\sum_\sigma \Delta\mathrm{T}_\sigma - 2[\hat{\mathrm{O}}(q_s\Delta\mathrm{T}_s) - \mathrm{P}_0\sum_\sigma(q_\sigma\Delta\mathrm{T}_\sigma)]\frac{\sum_\sigma(q_\sigma\Delta\mathrm{T}_\sigma)}{\sum_\sigma \mathrm{T}_\sigma^{00}}}\ , \\ S &= \frac{\sum_\sigma \mathrm{T}_\sigma^{00}}{(\sum_\sigma \mathrm{T}_\sigma^{00} + \sum_\sigma \Delta\mathrm{T}_\sigma) - \frac{[\sum_\sigma(q_\sigma\Delta\mathrm{T}_\sigma)]^2}{\sum_\sigma \mathrm{T}_\sigma^{00}}},\end{aligned}$$

where $\hat{\mathrm{O}}$ is an operator acting as, for example, for T_s and $s = \{c, \sigma\}$, $\hat{\mathrm{O}}\mathrm{T}_s = \{2\mathrm{Re}(\mathrm{T}_c), 2\mathrm{Im}(\mathrm{T}_c), \ominus\mathrm{T}_\sigma\}$, where $\ominus\mathrm{T}_\sigma = \mathrm{T}_\uparrow - \mathrm{T}_\downarrow$. The three components correspond to $\{\mathrm{P}_x, \mathrm{P}_y, \mathrm{P}_z\}$, respectively. The relations among the quantities p_i^{bg}, Q', $\mathrm{P}_{i,0}$, $\Delta\mathrm{P}_i$, and Q are

$$\begin{aligned}|p_i^{bg}|^2 &= P_{i,0}, \\ \mathrm{Re}(Q') &= \Delta\mathrm{P}_i Q/\mathrm{P}_{i,0}, \\ \mathrm{Im}(Q') &= \sqrt{1 + \Delta\mathrm{P}_i/\mathrm{P}_{i,0} - Q^2(\Delta\mathrm{P}_i/\mathrm{P}_{i,0})^2},\end{aligned}$$

where the parameter Q' governs the shape of the Fano resonance profile [1, 2, 11, 20]. In addition, Eq. (30) gives corrections of the peak position and of the width for the spin polarization vector [Eq. (29)] in comparison with those in T_σ and T_c. In particular, the new position and width are, respectively,

$$E'_\alpha = \mathrm{Re}(\varepsilon_\alpha) - \gamma_\alpha \frac{\sum_\sigma (q_\sigma \Delta\mathrm{T}_\sigma)}{\sum_\sigma \mathrm{T}_\sigma^{00}}, \tag{31}$$

$$\gamma'_\alpha = \gamma_\alpha/\sqrt{S}. \tag{32}$$

These corrections are typically insignificant. To demonstrate this point, we compare [56, 57] the peak positions and widths of various resonances by plotting the logarithm of the width, $\ln\gamma_\alpha$, versus $\mathrm{Re}(\epsilon_\alpha)$ for $\mathrm{T}_\uparrow$, P_z, and $|\mathbf{P}|$ as shown in Fig. 5. There are five resonance peaks, whose numerically obtained locations from Eq. (16) (marked by $\times$) can be compared with the theoretical predictions (marked by $\square$) from Eq. (20). For the same resonance peaks of $\mathbf{P}$, the corrected results from Eq. (32) for both the numerical [from Eq. (16), marked by +] and the theoretical [from Eq. (20), marked by $\bigcirc$] values are also included. It can be seen that the three types of results agree with each other well. Overall, these results represent strong evidence that both the spin polarization vector $\mathbf{P}$ and the spin-resolved transmission T_σ follow the Fano resonance profile.

C. Effect of dot geometry on Fano resonances in spin transmission and polarization

In general, in 2D spin transport, spin-resolved transmission and spin polarization depend on the dot structure [51], and the Fano resonance peaks arise due to the coupling between the quantum states in the lead and in the dot region. For example, when the Fermi energy is close to that of a bounded state in the corresponding closed dot region, the interaction between the propagating mode in the lead and the remnant of the bounded states in the

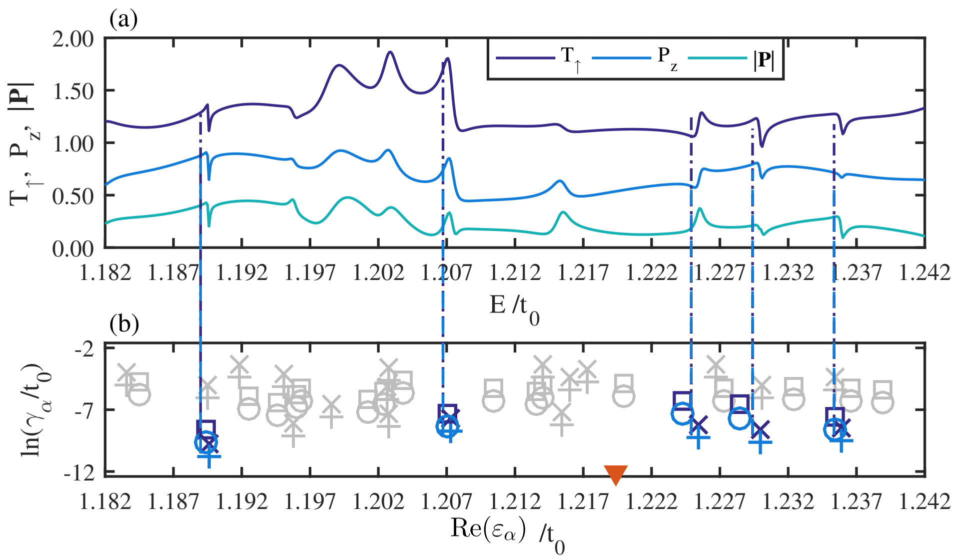

FIG. 5. *Comparison of Fano resonance widths obtained through numerics and theory for spin resolved transmission and spin polarization vector.* (a) Spin resolved transmission $T_\uparrow$, the z-component and magnitude of the polarization vector, P_z and $|\mathbf{P}|$, respectively, versus E in units of t_0. (b) Quantity $\ln(\gamma_\alpha/t_0)$ for $T_\uparrow$ and P_z or $|\mathbf{P}|$ versus $\mathrm{Re}(\varepsilon_\alpha)$. The symbols $\times$ and $\square$ denote the quantity $\ln(\gamma_\alpha/t_0)$, respectively, from Eqs. (16) and (20) for $T_\uparrow$. The symbols $+$ and $\bigcirc$ represent $\ln(\gamma_\alpha/t_0)$ in Eqs. (16) and (20), respectively, both being corrected by Eq. (32) for P_z or $|\mathbf{P}|$. The point $E_0 = 1.22t_0$ is marked as a red triangle ▼ on the horizontal axis of (b). For visualization purpose, the curve of P_z has been shifted up by 0.6 while others are unshifted.

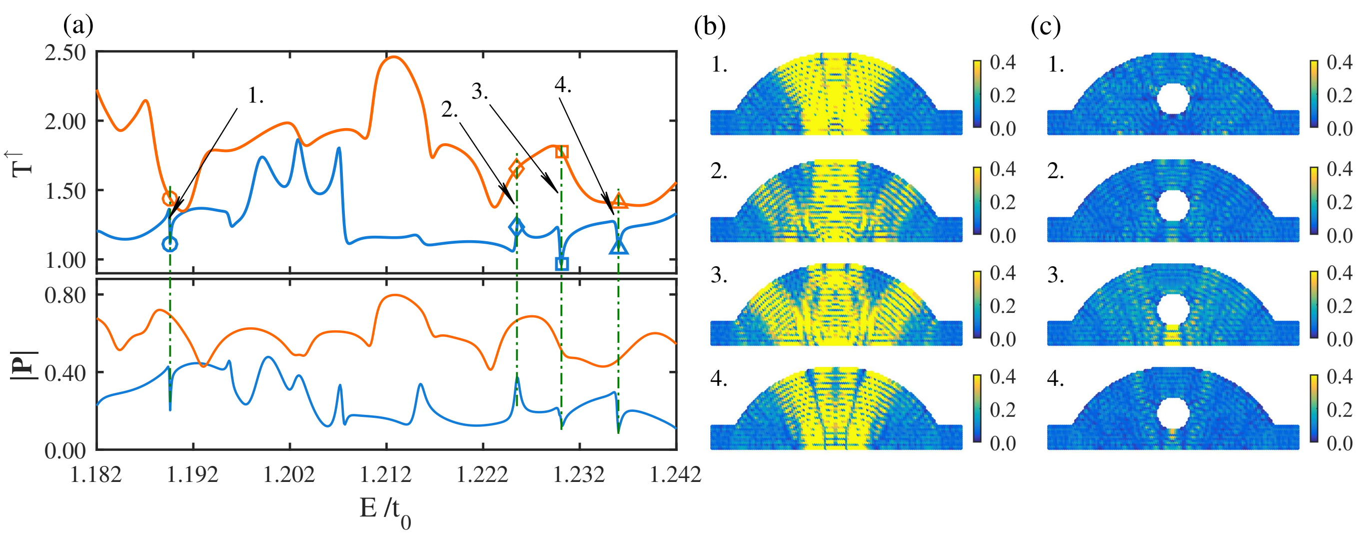

FIG. 6. *Shape dependence of spin transport.* (a) Spin-resolved transmission $T_\uparrow$ and the magnitude of the spin polarization vector $|\mathbf{P}|$ versus E in units of t_0 for a bow-shaped dot region are depicted - the lower curves. There are four peaks with their corresponding energy values marked by different symbols labeled as (1-4). The upper curves [shifted upward by 0.3 for both $T_\uparrow$ and $|\mathbf{P}|$] correspond to the same quantities but for a modified geometry of the dot region: there is a hard circle of radius $r = 0.2R$ located at the center of the original bow-shaped dot, into which waves are unable to penetrate. The original sharp Fano resonances have been smoothed out by alteration of the geometrical structure of the dot. (b,c) 2D maps of the density of states associated with the four peaks in (a) for the original bow-shaped dot and the modified dot structure with a central circular forbidden region, respectively. Associated with the original sharp resonances are strongly localized states in (b), whereas such states no longer exist for the modified dot.

open dot region will be strengthened, leading to a Fano resonance peak [2]. If we modify the geometric structure of the dot region, the original bound state at this energy will in general disappear, so will the Fano resonance. We expect this "washing out" effect or disappearance of resonances to occur for quantities underlying spin transport, especially spin-resolved transmission and the polarization vector.

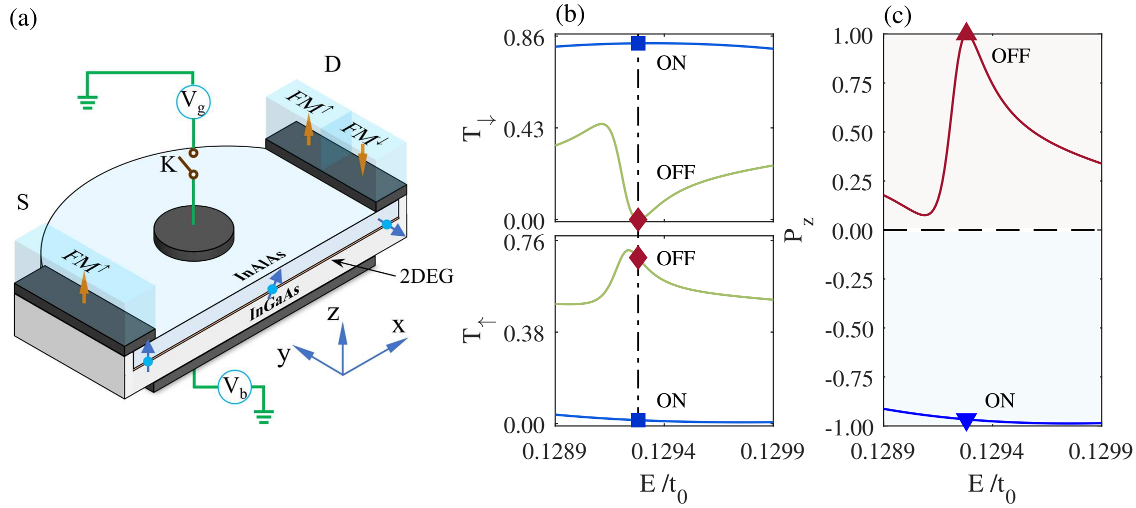

FIG. 7. *A scheme of electronic switch for spin transport.* (a) A schematic illustration of the proposed electronic switch device exploiting a spin Fano resonance. The device is a semiconductor heterostructure (e.g, $In_xGa_{1-x}As/In_yAl_{1-y}As$) [58]. Terminal-S is a ferromagnetic source that emits spin-↑ polarized electrons only, while terminal-D possesses two independent ferromagnetic drains that are able to detect either spin-↑ or -↓ polarized electrons. The back gate with V_b can be used to produce the Rashba electrical field. The circular gate inside the structure with $V_g < 0$ repels electrons, producing an effective circular forbidden region. (b) Spin-dependent transmission and $T_\downarrow$ $T_\uparrow$ versus E in units of t_0 in an interval covering a specific Fano resonance peak. For each quantity, two cases are plotted with either the switch on or off. (c) Spin polarization P_z versus E in the same range as in (b), which demonstrates the working of the switch: for $E/t_0 = 0.1293$ as marked by the symbols in (b) and (c), when the switch is on, $T_\uparrow$ is close to zero and $P_z \approx -1$, so the output current is almost purely associated with spin-down electrons. When the switch is off, $T_\downarrow = 0$ and $P_z = 1$, so that the output current constitutes purely spin-up electrons.

To demonstrate the effect of variations in the dot geometry on Fano resonances in spin transmission and polarization, we modify the dot structure by adding a hard circular disk at the center of the dot region. Figure 6 shows representative results. Especially, Fig. 6(a) shows the curves of $T_\uparrow$ (upper panel) and $|\mathbf{P}|$ (lower panel) for two cases: (i) unmodified dot structure of radius $R = 0.6\mu$m, cut-width $w = 0.7R$, lead with $h = 0.2R$ ($N = 12$ modes) - the lower blue curves, and (ii) modified dot structure with a central circular region removed (equivalent to a circular hard disk for electron waves and can be realized by applying a local gate potential draining out the electrons) - the upper orange curves. It can be seen that the four Fano resonance peaks labeled as (1-4) on the lower blue curves in the energy range are drastically smoothed out by the geometric modification of the dot structure. This effect can be further seen by examining the local density of state (LDOS) defined as [4]

$$\rho(\boldsymbol{r};E) = -\frac{1}{\pi}\mathrm{Im}[G^R(\boldsymbol{r},\boldsymbol{r};E)]. \tag{33}$$

Figures 6(b) shows the LDOS associated with the four Fano resonance peaks in the unmodified system, which exhibits a strongly localized behavior. For the same energy value, the localization no longer exists in the modified dot, signifying the disappearance of the original Fano resonances. A practical implication of the results in Fig. 6 is that spin transport and Fano resonances can be modulated through geometric modifications of the dot structure, which can be experimentally realized by applying a judiciously designed gate potential profile to the quantum dot [56, 57].

D. Electronic switch device for spin transport

Spin Fano resonances can be exploited for device applications. Here we present a design of an electronic switch that can control the spin orientation of the electrons associated with the output current. The basic structure of the device is a semiconductor heterostructure, as shown in Fig. 7(a), where the confining boundary has the shape shown in Fig. 1(a). A gate potential is applied to a circular region above the cavity with a controlling switch. When the switch is off, electrons move ballistically inside the cavity whose classical dynamics are mixed with stable periodic orbits, leading to sharp Fano resonances. When the switch is on so that a negative potential is applied, the electrons under the circular gate will be repelled out, forming effectively a circular forbidden region, as shown in Fig. 6(c), leading to drastic and characteristic changes in the underlying classical dynamics. As a result, the originally sharp Fano resonances will be either broadened or removed, generating distinct spin transport behaviors.

To explain the working of the device, we present a concrete example. In particular, we choose the Fermi energy to be $E/t_0 = 0.1293$, which corresponds to a spin Fano resonance. Figures 7(b) and 7(c) demonstrate that the output current can be controlled to either being made up of purely spin-up electrons (when the gate potential is off), or constituting almost purely spin-down electrons (with gate potential on). We see that the energy value for $T_\uparrow$ to reach a maximum and that for $T_\downarrow$ to become minimum are nearly identical but with a small difference. The reason is that, when $T_\uparrow$ takes on a maximum value, $T_\downarrow$ will no longer be zero but will have a small value, with their sum being one. Nevertheless, whether the gate voltage is off or on can cause the electrons constituting the output current to be either spin-up or spin-down, respectively. There are other Fano resonance peaks at which the gate potential can make the spin of the output electrons either polarized in the z-direction, where the value of P_z can be close to 1 or -1, or polarized in the $x-y$ plane where the value of P_z is close to zero. For different spin Fano resonances, the device can thus generate electrons with drastically different spin orientations.

IV. CONCLUSION AND DISCUSSION

We have generalized the universal Fano resonance formula describing quantities associated with electronic transport in 2D mesoscopic systems (e.g., conductance) to two key quantities underlying spin transport: spin-resolved transmission and spin polarization vector. The fact that Fano resonances, regardless of the nature of the transport (electronic or spin), are described by formulas of essentially the same form is strong indication of the same physics underlying the transport or scattering processes: Fano resonances are the result of the interaction between the continuous propagating states in the waveguide leads and the discrete states in the scattering region. While our analysis is of the perturbative type, where the self-energies describing the interactions are treated as a perturbation, the resonance peaks in the spin-resolved transmission and spin polarization vector predicted by two slightly different theories agree well not only with each other but also with those from direct numerical simulation, validating the analysis. We have also demonstrated that Fano resonances in spin transport can be smoothed out or even removed through geometrical modifications to the scattering region. We note that there were previous studies of control of quantum transport with respect to electronic properties [20, 22, 24, 25], especially the scheme of exploiting geometrical modification to modulate conductance fluctuations [56, 57]. Our results suggest that the same principle can be applied to spin transport. Especially, given that the Fermi energy takes on the value for a particular Fano resonance, by changing the nature of the classical dynamics, e.g., through a properly designed local gate potential, the resonance can be weakened or enhanced, leading to drastic changes in the spin transport properties. This effect can be exploited to design electronically controlled switches for spin transport, a key component in spintronic devices.

We wish to further clarify that our work was motivated by the fact that, while Fano resonances associated with electronic transport have been reasonably well understood, a systematic and quantitative understanding of spin Fano resonances was lacking. The goals of our study were to gain such an understanding and to design an electrically controlled switch for spin transport with an eye toward potential applications in spintronics. As explained, our understanding of how spin Fano resonances emerge naturally leads to a mechanism for their breakdown: localized states can be removed by altering the nature of the corresponding classical dynamics, and this has significance in practical applications.

It is generally true that the origin of the Fano resonance lies in the properties of the S-matrix, and any observable built from it should exhibit a Fano profile. However, to derive explicitly the resonance profiles for general physical observables is highly nontrivial. For example, as demonstrated in a previous work [5], even if the channel-to-channel scattering Fano profile is known, it is far from straightforward to obtain the overall resonance profile for the transmission. To derive the resonance profile for spin transport, we follow the standard method of decomposing the Greens function into a slow and a fast component, but the derivation is much more challenging and sophisticated than that without spin, making our analytic derivation a meaningful contribution to the field.

Broadly, Fano resonances are a common phenomenon in a large variety of quantum transport and scattering systems. The contribution of our work is that, for spin-resolved transport systems, not only can Fano resonances occur in the total current, but the spin resolved current and the spin polarization vector can also exhibit such resonances. From a theoretical point of view, we have developed a framework to generalize the conventional Green's function formalism to spin transport and employed the Fisher-Lee relation to obtain the spin resolved transmission matrix from which the spin polarization vector to be calculated. Treating the coupling to the leads as a perturbation and separating the Green's function into a slow and a fast component, we have succeeded in deriving explicit formulas for spin resonances. Our theory predicts that classical chaos can have a dramatic effect on the width of the spin Fano resonance, which has been verified numerically with a generic type of dot geometry that generates nonhyperbolic chaotic dynamics in the classical limit. Exploiting classical chaos also leads to a regularization scheme for spin-resolved transmission and spin polarization fluctuations with potential benefits to spintronics. To our knowledge, prior to our work, explicit formulas for spin Fano resonance did not exist. Furthermore, while there were previous studies on the effect of classical chaos on spin transport [51, 59–63], the understanding of how chaos helps remove or weaken spin Fano resonances was at a qualitative level. Our present work provides a quantitative understanding.

ACKNOWLEDGMENTS

This work was supported by NNSF of China under Grants No. 11775101, No. 11834005, and No. 11674139. YCL is supported by the Pentagon Vannevar Bush Faculty Fellowship program sponsored by the Basic Research Office of the Assistant Secretary of Defense for Research and Engineering and funded by the Office of Naval Research through Grant No. N00014-16-1-2828.

[1] U. Fano, "Effects of configuration interaction on intensities and phase shifts," Phys. Rev. **124**, 1866 (1961).

[2] A. E. Miroshnichenko, S. Flach, and Y. S. Kivshar, "Fano resonances in nanoscale structures," Rev. Mod. Phys. **82**, 2257 (2010).

[3] J. U. Nöckel and A. D. Stone, "Resonance line shapes in quasi-one-dimensional scattering," Phys. Rev. B **50**, 17415 (1994).

[4] S. Datta, *Electronic Transport in Mesoscopic Systems* (Cambridge University Press, Cambridge, England, 1995).

[5] T. Nakanishi, K. Terakura, and T. Ando, "Theory of Fano effects in an Aharonov-Bohm ring with a quantum dot," Phys. Rev. B **69**, 115307 (2004).

[6] S. Klaiman, N. Moiseyev, and H. R. Sadeghpour, "Interpretation of the Fano lineshape reversal in quantum waveguides," Phys. Rev. B **75**, 113305 (2007).

[7] R. Yang, L. Huang, Y.-C. Lai, and C. Grebogi, "Quantum chaotic scattering in graphene systems," Europhys. Lett. **94**, 40004 (2011).

[8] Y. Yoon, M.-G. Kang, T. Morimoto, M. Kida, N. Aoki, J. L. Reno, Y. Ochiai, L. Mourokh, J. Fransson, and J. P. Bird, "Coupling quantum states through a continuum: A mesoscopic multistate Fano resonance," Phys. Rev. X **2**, 021003 (2012).

[9] J. Fransson, M.-G. Kang, Y. Yoon, S. Xiao, Y. Ochiai, J. L. Reno, N. Aoki, and J. P. Bird, "Tuning the Fano resonance with an intruder continuum," Nano Lett. **14**, 788 (2014).

[10] I. Rotter and J. P. Bird, "A review of progress in the physics of open quantum systems: theory and experiment," Rep. Prog. Phys. **78**, 114001 (2015).

[11] L. Huang, Y.-C. Lai, H.-G. Luo, and C. Grebogi, "Universal formalism of Fano resonance," AIP Adv. **5**, 017137 (2015).

[12] S. M. Reimann and M. Manninen, "Electronic structure of quantum dots," Rev. Mod. Phys. **74**, 1283 (2002).

[13] F. A. Zwanenburg, A. S. Dzurak, A. Morello, M. Y. Simmons, L. C. L. Hollenberg, G. Klimeck, S. Rogge, S. N. Coppersmith, and M. A. Eriksson, "Silicon quantum electronics," Rev. Mod. Phys. **85**, 961 (2013).

[14] H. G. Luo, T. Xiang, X. Q. Wang, Z. B. Su, and L. Yu, "Fano resonance for Anderson impurity systems," Phys. Rev. Lett. **92**, 256602 (2004).

[15] A. P. S. de Moura, Y.-C. Lai, R. Akis, J. P. Bird, and D. K. Ferry, "Tunneling and nonhyperbolicity in quantum dots," Phys. Rev. Lett. **88**, 236804 (2002).

[16] W. H. Zurek, "Decoherence, einselection, and the quantum origins of the classical," Rev. Mod. Phys. **75**, 715 (2003).

[17] D. K. Ferry, R. Akis, and J. P. Bird, "Einselection in action: Decoherence and pointer states in open quantum dots," Phys. Rev. Lett. **93**, 026803 (2004).

[18] B. Huckestein, R. Ketzmerick, and C. H. Lewenkopf, "Quantum transport through ballistic cavities: Soft vs hard quantum chaos," Phys. Rev. Lett. **84**, 5504 (2000).

[19] E. R. Racec, U. Wulf, and P. N. Racec, "Fano regime of transport through open quantum dots," Phys. Rev. B **82**, 085313 (2010).

[20] A. A. Clerk, X. Waintal, and P. W. Brouwer, "Fano resonances as a probe of phase coherence in quantum dots," Phys. Rev. Lett. **86**, 4636 (2001).

[21] S. Katsumoto, "Coherence and spin effects in quantum dots," J. Phys-Condens. Mat. **19**, 233201 (2007).

[22] A. Bärnthaler, S. Rotter, F. Libisch, J. Burgdörfer, S. Gehler, U. Kuhl, and H.-J. Stöckmann, "Probing decoherence through Fano resonances," Phys. Rev. Lett. **105**, 056801 (2010).

[23] R. Yuan, R. Wang, Z. Duan, X. Song, B. Wang, and H. Yan, "Mesoscopic Fano effect modulated by Rashba spin-orbit coupling and external magnetic field," Phys. Lett. A **365**, 248 (2007).

[24] M. Mendoza, P. A. Schulz, R. O. Vallejos, and C. H. Lewenkopf, "Fano resonances in the conductance of quantum dots with mixed dynamics," Phys. Rev. B **77**, 155307 (2008).

[25] Y. Berlatzky and S. Klaiman, "Controlling Fano profiles via conical intersections," Phys. Rev. B **79**, 085303 (2009).

[26] I. Žutić, J. Fabian, and S. Das Sarma, "Spintronics: Fundamentals and applications," Rev. Mod. Phys. **76**, 323 (2004).

[27] A. Fert, "Nobel lecture: Origin, development, and future of spintronics," Rev. Mod. Phys. **80**, 1517 (2008).

[28] L. G. Mourokh, V. I. Puller, A. Y. Smirnov, and J. P. Bird, "Readout of single spins via Fano resonances in quantum point contacts," Appl. Phys. Lett. **87**, 192501 (2005).

[29] F. Chi, J.-L. Liu, and L.-L. Sun, "Fano-Rashba effect in a double quantum dot Aharonov-Bohm interferometer," J. Appl. Phys. **101**, 093704 (2007).

[30] W. Gong, Y. Zheng, Y. Liu, F. N. Kariuki, and T. Lu, "Fano effect in a T-shaped double quantum dot structure in the presence of Rashba spin-orbit coupling," Phys. Lett. A **372**, 2934 (2008).

[31] M. P. Nowak, B. Szafran, and F. M. Peeters, "Fano resonances and electron spin transport through a two-dimensional spin-orbit-coupled quantum ring," Phys. Rev. B **84**, 235319 (2011).

[32] M. E. Torio, K. Hallberg, S. Flach, and M. Miroshnichenko, A. E.and Titov, "Spin filters with Fano dots," Eur. Phys. J. B - Cond. Matt. Complex Sys. **37**, 399 (2004).

[33] J. F. Song, Y. Ochiai, and J. P. Bird, "Fano resonances in open quantum dots and their application as spin filters," Appl. Phys. Lett. **82**, 4561 (2003).

[34] V. V. Val'kov, S. V. Aksenov, and E. A. Ulanov, "Spin-flip induction of Fano resonance upon electron tunneling through atomic-scale spin structures," J. Exp. Theor. Phys. **116**, 854 (2013).

[35] G.-H. Ding and B. Dong, "Spin interference and the Fano effect in electron transport through a mesoscopic ring side-coupled with a quantum dot," J. Phys. Cond. Mat. **22**, 135301 (2010).

[36] R. Zhu, "Spin-dependent Fano resonance induced by a conducting chiral helimagnet contained in a quasi-one-dimensional electron waveguide," J. Phys. Cond. Mat. **25**, 036001 (2012).

[37] H.-H. Fu and K.-L. Yao, "Spin-filter and Fano antiresonant effect in conductance through a zigzaglike polymer device: Nonequilibrium Green's function approach," J. Chem. Phys. **134**, 054903 (2011).

[38] K. P. Wójcik and I. Weymann, "Perfect spin polarization in T-shaped double quantum dots due to the spin-dependent Fano effect," Phys. Rev. B **90**, 115308 (2014).

[39] Y.-C. Lai, R. Blümel, E. Ott, and C. Grebogi, "Quantum manifestations of chaotic scattering," Phys. Rev. Lett. **68**, 3491 (1992).

[40] R. Ketzmerick, "Fractal conductance fluctuations in generic chaotic cavities," Phys. Rev. B **54**, 10841 (1996).

[41] R. P. Taylor, R. Newbury, A. S. Sachrajda, Y. Feng, P. T. Coleridge, C. Dettmann, N. Zhu, H. Guo, A. Delage, P. J. Kelly, and Z. Wasilewski, "Self-similar magnetoresistance of a semiconductor Sinai billiard," Phys. Rev. Lett. **78**, 1952 (1997).

[42] A. S. Sachrajda, R. Ketzmerick, C. Gould, Y. Feng, P. J. Kelly, A. Delage, and Z. Wasilewski, "Fractal conductance fluctuations in a soft-wall stadium and a Sinai billiard," Phys. Rev. Lett. **80**, 1948 (1998).

[43] R. Crook, C. G. Smith, A. C. Graham, I. Farrer, H. E. Beere, and D. A. Ritchie, "Imaging fractal conductance fluctuations and scarred wave functions in a quantum billiard," Phys. Rev. Lett. **91**, 246803 (2003).

[44] X. Ni, L. Huang, L. Ying, and Y.-C. Lai, "Relativistic quantum tunneling of a Dirac fermion in nonhyperbolic chaotic systems," Phys. Rev. B **87**, 224304 (2013).

[45] Y.-C. Lai and T. Tél, *Transient Chaos: Complex Dynamics on Finite-Time Scales* (Springer, New York, 2011).

[46] L. D. Landau and E. M. Lifshitz, *Quantum Mechanics (Non-Relativistic Theory)*, 3rd ed. (World Publishing Company, New York, 2007).

[47] W. A. Lin and R. V. Jensen, "Conjugate points in stadium and circle billiards," Phys. Rev. E **56**, 5251 (1997).

[48] S. Ree and L. E. Reichl, "Classical and quantum chaos in a circular billiard with a straight cut," Phys. Rev. E **60**, 1607 (1999).

[49] B. K. Nikolić and S. Souma, "Decoherence of transported spin in multichannel spin-orbit-coupled spintronic devices: Scattering approach to spin-density matrix from the ballistic to the localized regime," Phys. Rev. B **71**, 195328 (2005).

[50] B. K. Nikoli and R. L. Dragomirova, "What can we learn about the dynamics of transported spins by measuring shot noise in spinorbit-coupled nanostructures?" Semicond. Sci. Tech. **24**, 064006 (2009).

[51] C.-R. Liu, X.-Z. Chen, H.-Y. Xu, L. Huang, and Y.-C. Lai, "Effect of chaos on two-dimensional spin transport," Phys. Rev. B **98**, 115305 (2018).

[52] E. Joos, H. D. Zeh, C. Kiefer, D. Giulini, J. Kupsch, and I. O. Stamatescu, *Decoherence and the Appearance of a Classical World in Quantum Theory* (Springer, Berlin Heidelberg, New York, 2003).

[53] M. Schlosshauer, *Decoherence and the Quantum-To-Classical Transition* (Springer, Berlin Heidelberg, New York, 2007).

[54] J.-Y. Zeng, *Liangzi lixue. Juan II. Diwuban [Quantum Mechanics. Volume II. 5th edition]* (Beijing: Kexue chubanshe, 2014).

[55] J. Sakurai and J. Napolitano, *Modern Quantum Mechanics* (Cambridge University Press, 2017).

[56] R. Yang, L. Huang, Y.-C. Lai, and L. M. Pecora, "Modulating quantum transport by transient chaos," Appl. Phys. Lett. **100**, 093105 (2012).

[57] R. Yang, L. Huang, Y.-C. Lai, C. Grebogi, and L. M. Pecora, "Harnessing quantum transport by transient chaos," Chaos **23**, 013125 (2013).

[58] F. Mireles and G. Kirczenow, "Ballistic spin-polarized transport and rashba spin precession in semiconductor nanowires," Phys. Rev. B **64**, 024426 (2001).

[59] Y. V. Pershin and V. Privman, "Low spin relaxation in two-dimensional electron systems with antidots," Phys. Rev. B **69**, 073310 (2004).

[60] C. H. Chang, A. G. Mal'shukov, and K. A. Chao, "Spin relaxation dynamics of quasiclassical electrons in ballistic quantum dots with strong spin-orbit coupling," Phys. Rev. B **70**, 245309 (2004).

[61] F. Zhai and H. Q. Xu, "Symmetry of spin transport in two-terminal waveguides with a spin-orbital interaction and magnetic field modulations," Phys. Rev. Lett. **94**, 246601 (2005).

[62] G. B. Akguc and J.-B. Gong, "Spin-dependent electron transport in two-dimensional waveguides of arbitrary geometry," Phys. Rev. B **77**, 205302 (2008).

[63] L. Ying and Y.-C. Lai, "Enhancement of spin polarization by chaos in graphene quantum dot systems," Phys. Rev. B **93**, 085408 (2016).